applied sciences

MDPI

Article

Pressure Transient Model of Water-Hydraulic Pipelines with Cavitation

Dan Jiang *, Cong Ren, Tianyang Zhao and Wenzhi Cao

School of Mechanical and Electrical Engineering, University of Electronic Science and Technology of China, Chengdu 611731, China; congR0420@163.com (C.R.); zty1990321@gmail.com (T.Z.); wenzhicao2014@gmail.com (W.C.)

* Correspondence: jdan2002@uestc.edu.cn

Received: 15 February 2018; Accepted: 1 March 2018; Published: 7 March 2018

Abstract: Transient pressure investigation of water-hydraulic pipelines is a challenge in the fluid transmission field, since the flow continuity equation and momentum equation are partial differential, and the vaporous cavitation has high dynamics; the frictional force caused by fluid viscosity is especially uncertain. In this study, due to the different transient pressure dynamics in upstream and downstream pipelines, the finite difference method (FDM) is adopted to handle pressure transients with and without cavitation, as well as steady friction and frequency-dependent unsteady friction. Different from the traditional method of characteristics (MOC), the FDM is advantageous in terms of the simple and convenient computation. Furthermore, the mechanism of cavitation growth and collapse are captured both upstream and downstream of the water-hydraulic pipeline, i.e., the cavitation start time, the end time, the duration, the maximum volume, and the corresponding time points. By referring to the experimental results of two previous works, the comparative simulation results of two computation methods are verified in experimental water-hydraulic pipelines, which indicates that the finite difference method shows better data consistency than the MOC.

Keywords: water-hydraulic pipelines; pressure transients; cavitation; finite difference method; method of characteristics

1. Introduction

Transient pressure pulsations generated by the rapid closure of a valve would easily cause hydraulic pipeline systems to burst because the pressure pulsations exceed the safe operating range of such pipelines. Violent pressure pulsations result in cavitation growth and collapse in these systems. To study the mechanism of cavitation during pressure transient pulsations, it is necessary to investigate the cavitation appearance, its volume evaluation, and the effect on the pipeline and hydraulic systems.

Pressure transients with cavitation in pipelines have been investigated by many researchers. Kojima et al. [1] presented the gas-nonbubbly flow model to predict pressure increments, which involved cavitation on the downstream side of the pipeline as a valve was instantaneously closed. They used a water–glycol mixture and an oil/water emulsion fluid including mineral oil as working fluids and compared the computed pressure pulsations with experimental results. Chaudhry et al. [2,3] then proposed a MacCormack scheme and a Gabutti scheme for pressure transient analysis, which was verified both in computed simulation and experimental studies. Although modeling accuracy was achieved, discrepancies in the pressure magnitudes between simulations and experiments were found. Transient pressure pulsations often lead to unexpected chatter, overshooting, and a zero bias of tracking error in the electrohydraulic control system [4–7]. Shu et al. [8–10] developed a vaporous cavitation model that used a two-phase homogeneous equilibrium to simulate pipeline pressure transients with upstream, midstream, and downstream cavitation. Bergant et al. [11,12] discussed three cavitation models: the discrete vapor cavity model (DVCM), the discrete gas cavity model (DGCM), and the generalized

interface vaporous cavitation model (GIVCM). The comparative results of the three cavitation models indicated that the GIVCM was able to directly obtain the regions of vaporous cavitation occurrence. Jiang et al. [13–16], via genetic algorithms, developed the parametric identification of the gas bubble model and the frequency-dependent friction model. Parametric identification and noise suppression are also addressed in mechanical ventilation [17–20]. Sadafi et al. [21] recently studied water hammers with cavitation in a simple reservoir-pipeline-valve system and a pumping station. Karadžić et al. [22] verified the robustness of the DGCM via analysis of the experimental results. Iglesias-Rey et al. [23] performed a detailed study of the actual behavior of different valves (both air intake and exhaust) and described the mathematical characterization of different commercial valves. Fuertes-Miquel et al. [24] presented a numerical modeling of pipelines with air pockets and air valves to study the behavior of the air inside pipes as the air was expelled through air valves. Majd et al. [25] investigated the unsteady flow of a non-Newtonian fluid due to the instantaneous valve closure in a pipeline. Comparison revealed a remarkable deviation in pressure history and velocity profile with respect to the water hammer in Newtonian fluids. Zhou et al. [26] adopted a second-order finite volume method for cavitation in the water column separation of pipelines to capture vapor cavities and predict their growth and collapse. Wang et al. [27] adopted a two-dimensional CFD model to characterize liquid column separation. The simulation results revealed the formation of an intermediate cavity and both the location and shape of the region undergoing distributed vaporous cavitation. Himr [28] also studied water hammers with column separation as a one-dimensional flow. The volume of the cavity was determined by Gibson's method, and the air bubbles were considered to affect the speed of sound.

Thanks to the research development of transient pressure in the fluid transmission field, the main contributions of this paper are as follows:

(i) Different from [10], a pressure transient model of water-hydraulic pipelines is constructed to reveal both the transient pressure magnitude and the dynamic characteristics of cavitation volume. To the authors' best knowledge, there have been few attempts to predict cavitation volume changes and illustrate its influence on pressure transients in hydraulic pipelines, as described in [14,15]. Although the simplified cavitation model is based on a flow continuity principle [29], the frictional force in pipelines involving the steady friction force and the frequency-dependent unsteady friction should be a primary consideration in pressure transient analysis.

(ii) Different from the MOC, the FDM is adopted to estimate the magnitudes of the pressure peaks and the changes in cavitation volume to adapt the transient pressure both with and without cavitation. Simultaneously, the respective boundary conditions of both the upstream and downstream sides of the valve are also considered. A comparison with the MOC is made; results are verified by the percentage of the integral of the absolute difference (IAD) between simulation and experimental reference results.

2. Mathematical Models

2.1. Basic Equations without Cavitation

The simple water-hydraulic pipe is shown in Figure 1. To illustrate the propagation and reflection of the pressure transients, the sequence of events, which is caused by a valve closure in the middle of the pipe connected with the downstream and upstream tanks, will be discussed. Without a loss of generality, the pipe diameter is assumed to be constant, and the released gas is negligible.

The general model of pressure transients in the pipeline involves the continuity equation and the momentum equation, which are mentioned in Wylie et al. [29]. The continuity equation is derived from the mass conservation law as follows:

$$\frac{1}{c_0^2}\frac{\partial p}{\partial t} + \frac{\rho}{\pi r_0^2}\frac{\partial q}{\partial x} = 0, \tag{1}$$

where p is the pressure in pipeline, q is the flow rate, ρ is the density of fluid, c_0 is the acoustic velocity in the fluid, r_0 is the radius of the pipeline, x is the spatial variable, and t is the time variable.

Meanwhile, the equation of momentum is constructed by Newton's law of motion as follows:

$$\frac{\rho}{\pi r_0^2}\frac{\partial q}{\partial t} + \frac{\partial p}{\partial x} + F(q) = 0. \tag{2}$$

In Equation (1), c_0 can be given by

$$c_0 = \sqrt{B_{eff}/\rho}, \tag{3}$$

where B_{eff} is the effective bulk modulus.

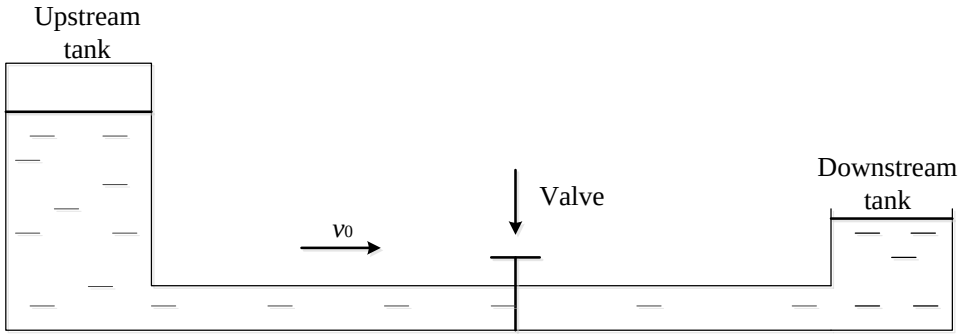

Figure 1. Tank-pipeline-valve system.

2.2. Continuity Equation under Vaporous Cavitation Condition

The cavitation normally arises when the pressure transients in pipelines are closed to the vapor pressure. If the pressure in the pipeline drops to or below the vapor pressure, vapor cavitation will form. Furthermore, if the pressure stays at the level of the vapor pressure and the cavitation size has approached a critical diameter, the cavitation will continue to grow rapidly. However, the cavitation will be unstable and collapse until the pressure is greater than the vapor pressure.

Pettersson et al. [30] and Harris et al. [31] presented a relatively simple cavitation model that illustrates the dynamic characteristics of piston pumps and can capture the key aspects of cavitation. Since the pressure in the pipeline element is assumed to be the vapor pressure under a vaporous cavitation condition, according to the flow continuity principle, the dynamics of the cavitation volume V_{cav} is given by

$$\frac{dV_{cav}}{dt} = q_{out} - q_{in}, \tag{4}$$

where q_{out} and q_{in} are the outflow rate and inflow rate of an element in the pipe, respectively.

2.3. Frictional Items

Due to the fluid viscosity, the frictional force $F(q)$ in Equation (2) can be described as the sum of the steady friction item and the frequency-dependent unsteady friction item. Zielke [32] considered the frequency-dependent friction item as some weighting functions described in the frequency domain via Laplace transform. Subsequently, Trikha [33] proposed three exponent function items to estimate the frequency-dependent friction. Then, Taylor et al. [34] optimized the coefficients of the Trikha model and proposed an approximate model with four exponent function items as follows:

$$F(q) = F_0 + \frac{1}{2}\sum_{i=1}^{4} Y_i, \tag{5}$$

where the first item F_0 is the steady friction, and the second item is the frequency-dependent unsteady friction. Based on the Darcy–Weisbach equation, F_0 can be expressed as

$$F_0 = \frac{\rho f v |v|}{4 r_0}. \tag{6}$$

The four items of frequency-dependent friction Y_i can be computed by

$$\begin{cases} \dfrac{\partial Y_i}{\partial t} = -\dfrac{n_i \mu}{\rho r_0^2} Y_i + m_i \dfrac{\partial F_0}{\partial t} \\ Y_i(0) = 0 \end{cases}, \quad i = 1, \ldots, 4 \tag{7}$$

where the constants n_i and m_i are listed in Table 1.

Table 1. n_i and m_i.

i	1	2	3	4
n_i	3.9479×10^1	2.9829×10^2	2.2279×10^3	8.8782×10^4
m_i	2.0141	5.3946	1.6259×10^1	3.2048×10^2

3. Simulation Methods

Two predictive methods, i.e., MOC and FDM, are presented. In order to solve the two partial differential equations in terms of pressure and flow rate, the pipeline is divided into n elements of equal length $\Delta x = L/n$, where L is the pipeline length. It should be noted that different test values of the pipeline length L can be selected in simulation. The FDM is implemented to describe pressure transients on the downstream and upstream sides of the valve, respectively.

3.1. Method of Characteristics

The continuity equation (Equation (1)) should be solved together with the momentum equation (Equation (2)) since they are partial differential forms about the two unknown parameters p and q. However, via the MOC, they can be transformed into ordinary differential equations (Equations (8) and (9)) along the characteristic lines C^+ and C^-.

$$C^+ : \begin{cases} \dfrac{\rho c_0}{\pi r_0^2} \dfrac{dq}{dt} + \dfrac{dp}{dt} + c_0 F(q) = 0 \\ \dfrac{dx}{dt} = c_0 \end{cases} \tag{8}$$

$$C^- : \begin{cases} \dfrac{\rho c_0}{\pi r_0^2} \dfrac{dq}{dt} - \dfrac{dp}{dt} + c_0 F(q) = 0 \\ \dfrac{dx}{dt} = -c_0 \end{cases}. \tag{9}$$

As shown in Figure 2, the pressure and flow rate values at points A (p_A and q_A) and B (p_B and q_B) are known. Integrating Equations (8) and (9) along the characteristic lines C^+ and C^-, the following Equation (10) is obtained to further derive the pressure and flow rate at point P (p_P and q_P).

$$\begin{cases} \dfrac{\rho}{\pi r_0^2} q_P + \dfrac{1}{c_0} p_P = \dfrac{\rho}{\pi r_0^2} q_A + \dfrac{1}{c_0} p_A - \dfrac{\Delta x}{c_0} F(q_A) \\ \dfrac{\rho}{\pi r_0^2} q_P - \dfrac{1}{c_0} p_P = \dfrac{\rho}{\pi r_0^2} q_B - \dfrac{1}{c_0} p_B - \dfrac{\Delta x}{c_0} F(q_B) \end{cases}. \tag{10}$$

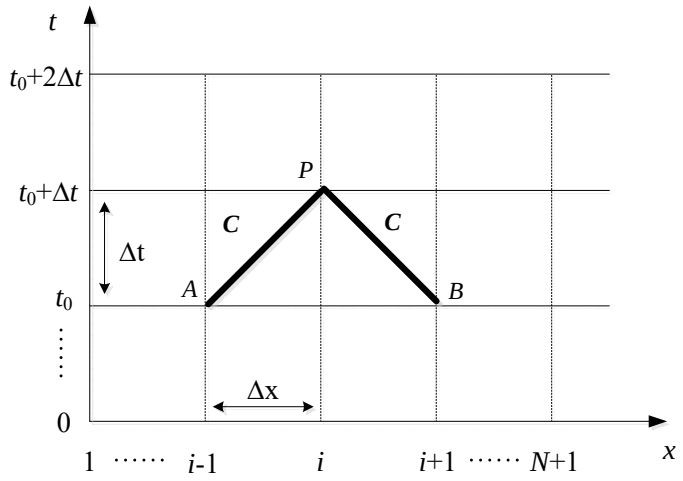

Figure 2. Method of characteristics.

Then, from Equation (10), the values of p_P and q_P can be obtained by

$$\begin{cases} p_P = \dfrac{c_0}{2} C_L - C_R \\ q_P = \dfrac{\pi r_0^2}{2\rho} C_L + C_R \end{cases}, \tag{11}$$

where

$$\begin{cases} C_L = \dfrac{\rho}{A} q_A + \dfrac{1}{c_0} p_A - \dfrac{\Delta x}{c_0} F(q_A) \\ C_R = \dfrac{\rho}{A} q_B - \dfrac{1}{c_0} p_B - \dfrac{\Delta x}{c_0} F(q_B) \end{cases}. \tag{12}$$

Details of the MOC are given by Wylie et al. [29] and Chaudhry et al. [3]. Incorporated with Equation (4), this method determines the time at which cavitation first arises in respective elements and the volume of cavitation. Furthermore, the method also determines whether cavitation has already collapsed at each time step $\Delta t = \Delta x / c_0$ and the time at which cavitation occurs again.

3.2. Finite Difference Method

The flow rate and pressure inside the pipeline are constructed as n-dimensional vectors as follows: $q = (q_1, q_2, \ldots, q_n)^{\mathrm{T}}$, and $p = (p_1, p_2, \ldots, p_n)^{\mathrm{T}}$. Here, the first element is close to the valve and the last element approaches the upstream or downstream tank. This simulation scheme has been implemented by the Matlab/Simulink platform and the partial derivative terms in time domain $\partial/\partial t$ can be readily calculated by the integral block of Simulink.

3.2.1. The Downstream Side of the Valve

Pressure transients on the downstream side of the valve were investigated. The sketch is illustrated in Figure 3. Here, the initial velocity v_0 is constant and the valve is suddenly shut off. For the boundary condition, the flow rate in the element close to the valve is set to zero, and the pressure in the element close to downstream tank is constant. If the boundary condition $q_{valve} = 0$ is assumed to be the first element together with the other $n - 1$ elements, the Selector Block is used to re-order specified elements of the vector. A new flow rate vector q' for the case of the flow rate is formed such that

$$q' = (q_{valve}, q_1, \ldots, q_{n-1})^{\mathrm{T}}. \tag{13}$$

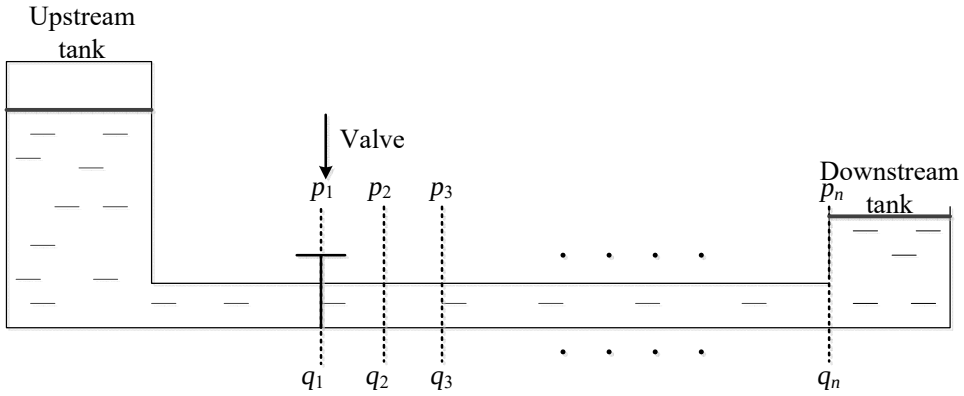

Figure 3. On the downstream side of a valve.

Based on the first-order upwind difference scheme, the derivative item $\partial q/\partial x$ can be expressed as follows:

$$\frac{\partial q}{\partial x} = \frac{q - q'}{\Delta x}. \tag{14}$$

For the pressure vector, the Selector Block is used to construct a new pressure vector p' as follows:

$$p' = (p_2, \ldots, p_n, p_{resd})^{\mathrm{T}}, \tag{15}$$

where p_{resd} is the boundary condition, which is equal to the pressure in the downstream tank.

$\partial p/\partial x$ is also given by

$$\frac{\partial p}{\partial x} = \frac{p' - p}{\Delta x}. \tag{16}$$

3.2.2. The Upstream Side of the Valve

Similar to the downstream side of the valve, an upstream pipeline model can be constructed. The variables of flow rate and pressure in n elements along the pipeline are considered as the vectors as shown in Figure 4. The first element is close to the valve, and the initial velocity is positive constant. For the case of the flow rate, a new flow rate vector q' is formed with the corresponding boundary condition, such that

$$q' = (q_{valve}, q_1, \ldots, q_{n-1})^{\mathrm{T}}. \tag{17}$$

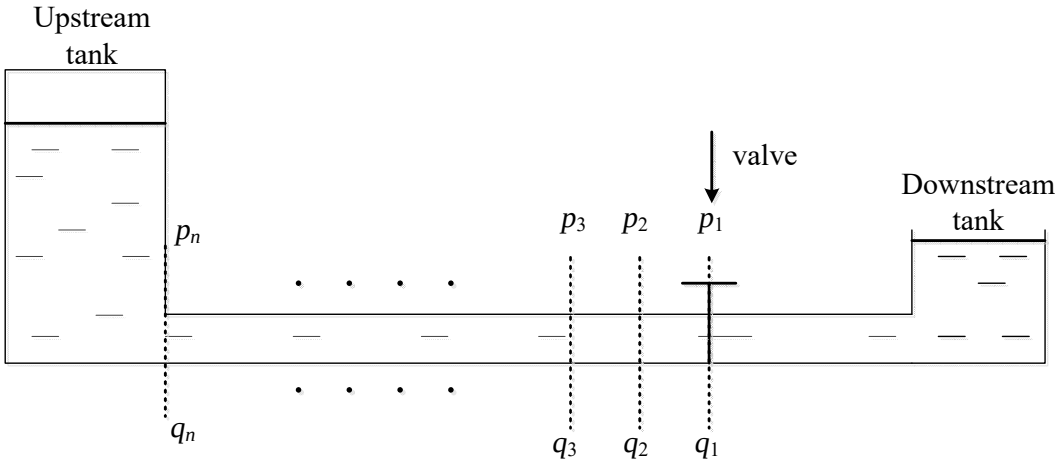

Figure 4. On the upstream side of a valve.

Different from the condition of the downstream side of the valve, according to the first-order upwind difference scheme, $\partial q/\partial x$ can be expressed as follows:

$$\frac{\partial q}{\partial x} = \frac{q' - q}{\Delta x}. \tag{18}$$

For the pressure vector, the Selector Block is used to create a new pressure vector p':

$$p' = (p_2, \ldots, p_n, p_{resu})^{\mathrm{T}}, \tag{19}$$

where p_{resu} is the boundary condition of the pressure in the upstream tank. Thus, the $\partial p/\partial x$ can be described as follows:

$$\frac{\partial p}{\partial x} = \frac{p - p'}{\Delta x}. \tag{20}$$

4. Simulation Results

4.1. Case 1: Pressure Transients without Cavitation on the Downstream Side of Valve

The experimental results of the transient pressure pulsations close to the valve in the horizontal downstream pipeline are given by Vitkovsky et al. [35] and the related parameters of the tested pipeline are listed in Table 2. Here, the element number n is selected as 30 in the simulation. The sensitivity of this element number n has been discussed in [13]. The corresponding experimental results of transient pressure pulsations close to the valve are shown as the solid line in Figure 5.

Table 2. Parameters of pressure transients without cavitation on the downstream side of the valve.

Parameter	Value
Upstream tank pressure p_{resu} (bar)	4.25
Downstream tank pressure p_{resd} (bar)	4.22
Pipe radius r_0 (mm)	11.05
Pipe length L (m)	37.2
Water density ρ (kg/m^3)	1000
Initial velocity v_0 (m/s)	0.3
Acoustic velocity in the fluid c_0 (m/s)	1319

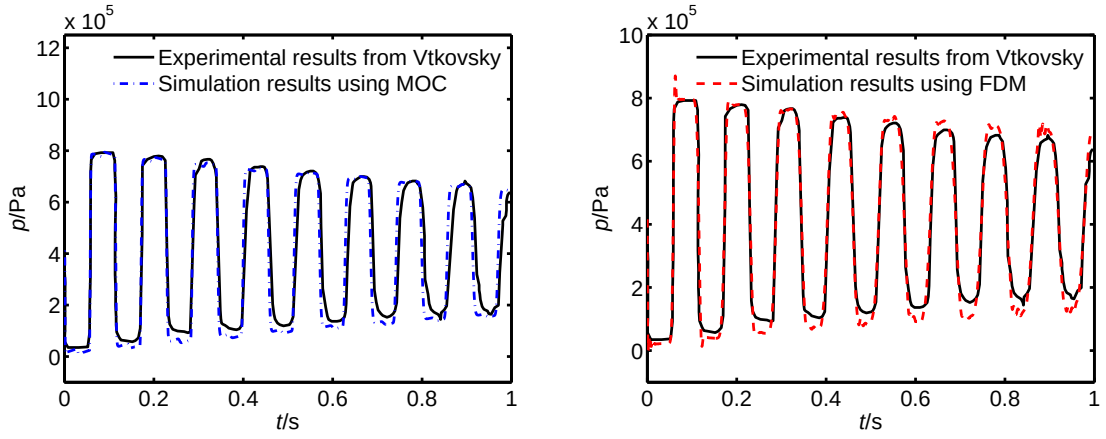

(**a**) Pressure transients results of the MOC (**b**) Pressure transients results of the FDM

Figure 5. Simulation and experimental pressure transients without cavitation on the downstream side of the valve.

Figure 5 denotes that, in the downstream pipeline, the pressure at the vicinity of the valve is reduced quickly when the valve is closed. At the same time, the negative pressure wave propagates to

the downstream tank. Then, the positive pressure wave is reflected from the downstream tank and travels back to the valve, which leads to the first positive pressure peak. This process may be repeated several times before the fluid energy is dissipated due to the frictional force of the pipeline.

As shown in the experimental results, from 0 to 1 s, the attenuated peaks of the pressure pulsations are decreased very slowly. Because of the lower frictional force, the magnitudes of the pressure peaks decay slower in water, which is different from the corresponding pressure transient results with the working fluid as hydraulic oil (Jiang et al. [13]). Thus, if the pressure pulsations are always greater than the saturated vapor pressure, no cavitation forms.

For comparison, the simulation results of MOC are illustrated as the dash-dotted line in Figure 5a. The simulation results of the FDM platform are presented as the dashed line in Figure 5b. It can be seen that, from 0.4 to 1 s, the phase difference between the MOC simulation and the experimental results is more obvious. However, the simulation results of the FDM are still consistent with the experimental pressure results.

To further compare the two predictive methods, the error between the simulation and the experimental results was evaluated by the percentage of the integral of absolute difference (IAD) as follows (Rabie et al. [36]):

$$IAD = \frac{\int_0^T \left| p_{Lth} - p_{L\exp} \right| dt}{p_{Lss} T} \times 100\%. \quad (21)$$

The IAD results of the two predictive methods in the three cases are listed in Table 3. In Case 1, the final steady-state pressure at the valve is equal to the downstream tank pressure (4.22 bar), and the IAD of the FDM is about 0.05%. Thus, the simulation of the FDM is consistent with the experimental result, which is superior to the MOC (IAD = 0.91%).

Table 3. The integral of absolute difference (IAD) of the method of characteristics (MOC) and the finite difference method (FDM).

Case	p_{Lss} (bar)	IAD of MOC	IAD of FDM
1	4.22	0.91%	0.05%
2	0.98065	2.75%	2.47%
3	4.90325	12.39%	10.84%

4.2. Case 2: Pressure Transients with Cavitation on the Downstream Side of Valve

The case of transient pressure pulsations with cavitation in the horizontal downstream pipeline was also investigated. Some experimental parameters from Sanada et al. [37] are listed in Table 4. The corresponding experimental results are shown as the solid line in Figure 6. As the valve is quickly closed, the pressure reduces and stays at vapor pressure for about 3 s. The pressure then drops again and stays at vapor pressure for about 1.5 s. For the third time, the pressure falls and stays at vapor pressure for about 1 s.

Table 4. Parameters of pressure transients with cavitation on the downstream side of the valve.

Parameter	Value
Upstream pressure p_{resu} (bar)	6.55164
Downstream pressure p_{resd} (bar)	0.98065
Pipe radius r_0 (mm)	7.6
Pipe length L (m)	200
Water density ρ (kg/m^3)	1000
Initial velocity v_0 (m/s)	1.5
Viscosity of the fluid c_0 (cP)	1

The results obtained from the MOC and the FDM are also shown in Figure 6. It is clear that obvious differences exist between the MOC simulation and the experimental results, especially in terms of the phase differences of the subsequent peaks. However, the results of the FDM via Matlab/Simulink Platform are consistent with the experimental results.

As listed in Table 3, for Case 2, the final steady-state pressure at the valve is 0.98065 bar, which is equal to the downstream tank pressure. Different from Case 1, the two predictive methods have similar effects (the IADs of the two predictive methods are 2.75% and 2.47%).

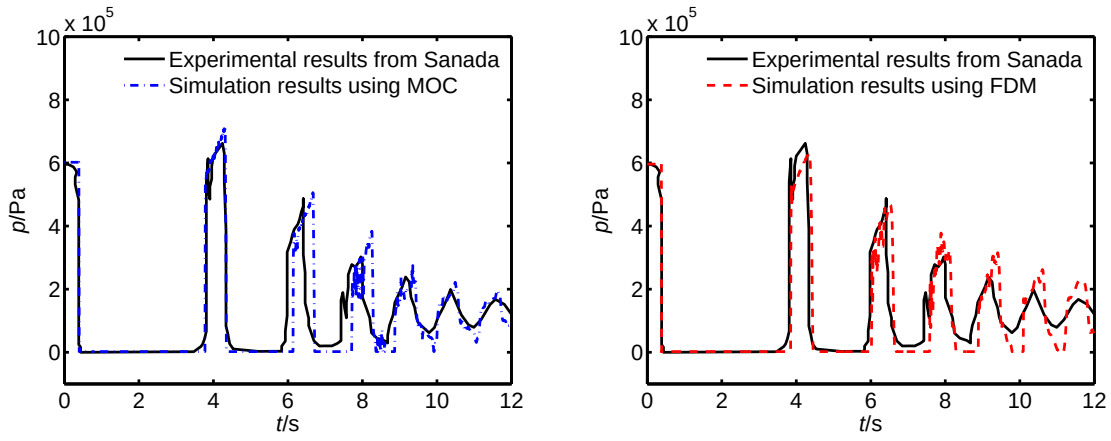

(**a**) Pressure transients results of the MOC (**b**) Pressure transients results of the FDM

Figure 6. Simulation results and experimental data of pressure transients with cavitation on the downstream side of the valve.

The corresponding cavitation volumes in the element close to the valve predicted by the FDM and the MOC are shown in Figure 7. The trends of vaporous cavitation volume under three cases are listed in Table 5, which includes the cavitation start time, the end time, the duration, the maximum volume, and the corresponding time points.

Similar to the MOC, the FDM is also able to track the trends of cavitation volume. The results indicate that the computed pressure peak declines to the saturated vapor pressure after the valve is rapidly closed and after cavitation forms. However, this new cavitation collapses at 3.87 s (FDM) and 3.77 s (MOC). The maximum volumes of cavitation first are 1.372×10^{-4} m^3 (FDM) and 1.401×10^{-4} m^3 (MOC). When the pressure declines again, cavitation is generated again, but it is much smaller (1.892×10^{-5} m^3 from the FDM and 4.155×10^{-5} m^3 from the MOC) than the first instance. Once again, cavitation collapses at the arrival of the third pressure peak. The durations of the third cavitation is 1.08 s (FDM) and 0.99 s (MOC). Thus, over this short period (12 s), the cavitation demonstrates generation and collapse three times.

Table 5. Trends of cavitation volume.

Times	Method	MOC (case 1)	FDM (case 1)	MOC (case 2)	FDM (case 2)	MOC (case 3)	FDM (case 3)
1st time	start time (s)	–	–	0.40	0.38	0.60	0.65
	end time (s)			3.77	3.87	1.21	1.24
	duration (s)			3.37	3.49	0.61	0.59
	maximum volume time (s)			2.32	2.11	1.08	1.21
	maximum volume (m^3)			1.401×10^{-4}	1.372×10^{-4}	1.305×10^{-5}	3.955×10^{-6}
2nd time	start time (s)	–	–	4.34	4.37	2.05	1.98
	end time (s)			6.14	6.03	2.17	2.23
	duration (s)			1.80	1.66	0.12	0.25
	maximum volume time (s)			5.12	5.73	2.15	2.21
	maximum volume (m^3)			4.155×10^{-5}	1.892×10^{-5}	1.281×10^{-6}	6.785×10^{-7}
3rd time	start time (s)	–	–	6.72	6.54		
	end time (s)			7.71	7.62		
	duration (s)			0.99	1.08	–	–
	maximum volume time (s)			7.46	6.76		
	maximum volume (m^3)			1.009×10^{-5}	1.535×10^{-6}		

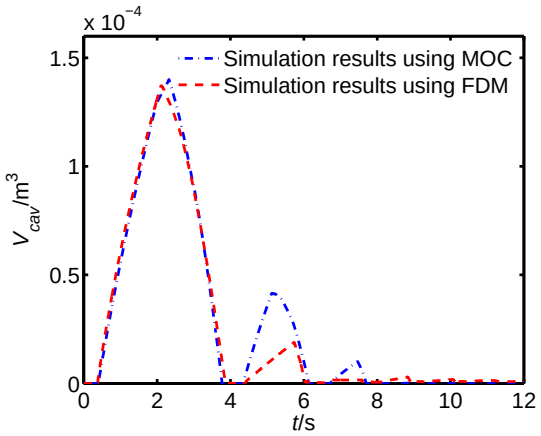

Figure 7. Simulation results of the cavitation volume in the first element on the downstream side of the valve using the MOC and the FDM.

4.3. Case 3: Pressure Transients with Cavitation on the Upstream Side of the Valve

Sanada et al. [37] also provided parameters of tested pipelines in the case of transient pressure pulsations in a horizontal upstream pipeline, as listed in Table 6. Compared with Case 2 listed in Table 4, the parameters of the test pipeline are the same, except for the values of the upstream pressure and the initial velocity.

Table 6. Parameters of pressure transients with cavitation on the upstream side of the valve.

Parameter	Value
Upstream pressure p_{resu} (bar)	4.90325
Downstream pressure p_{resd} (bar)	0.98065
Pipe radius r_0 (mm)	7.6
Pipe length L (m)	200
Water density ρ (kg/m^3)	1000
Initial velocity v_0 (m/s)	1.45
Viscosity of fluid c_0 (cP)	1

Figure 8 demonstrates the sequence of pressures with cavitation caused by instant valve closure. Compared with the pressure pulsations in the downstream pipeline, after a sudden valve closure, the fluid is brought to rest, firstly causing a high pressure peak at the upstream side of the valve.

Experimental results from Sanada (the solid line in Figure 8) show that the initial pressure at the valve is about 16×10^5 Pa when the valve is closed. It then reduces to the vapor pressure and keeps a steady state until about 0.5 s. Upon collapse of the cavitation, another pressure wave is generated at the valve. The subsequent pressure peak is reduced because of the friction force in the pipeline.

The figure also shows the simulation results from the MOC and the FDM. For the case of the upstream side of the valve, the final steady-state pressure at the valve is equal to the upstream tank pressure (4.90 bar). As listed in Table 3, the IADs of the MOC and the FDM are 12.39% and 10.84%. It is clear that the results of the FDM has much better consistency with the experimental results than those using the MOC.

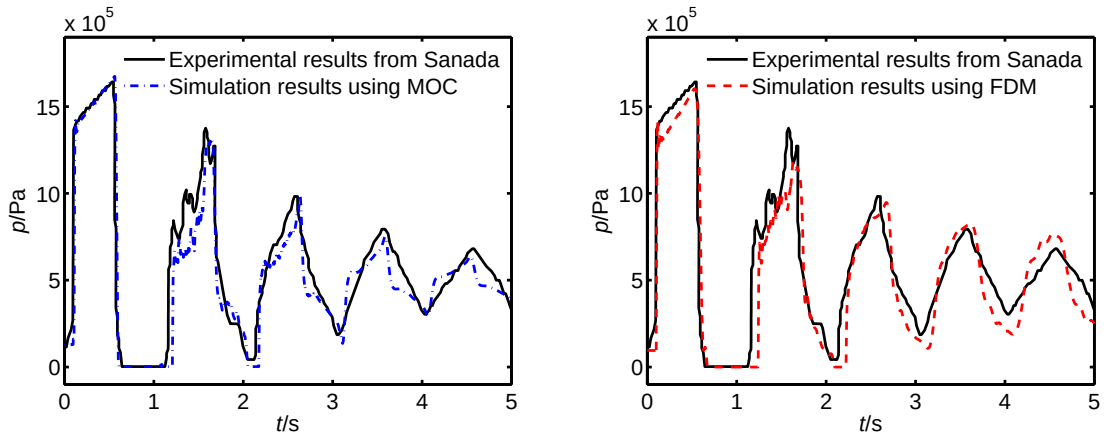

(**a**) Pressure transients results of the MOC (**b**) Pressure transients results of the FDM

Figure 8. Simulation results and experimental data of pressure pulsations on the upstream side of the valve.

The corresponding cavitation volumes in the element close to the valve are shown in Figure 9. The maximum size of the vaporous cavity is 3.955×10^{-6} m^3 (the duration is about 0.59 s) using the FDM and 1.305×10^{-5} m^3 (the duration is about 0.61 s) using the MOC. When the pressure reduces to vapor pressure again, using the FDM, the second cavity has a volume of 6.785×10^{-7} m^3 and a duration of 0.25 s; however, using the MOC, the cavity has a volume of 1.281×10^{-6} m^3 and a duration of 0.12 s.

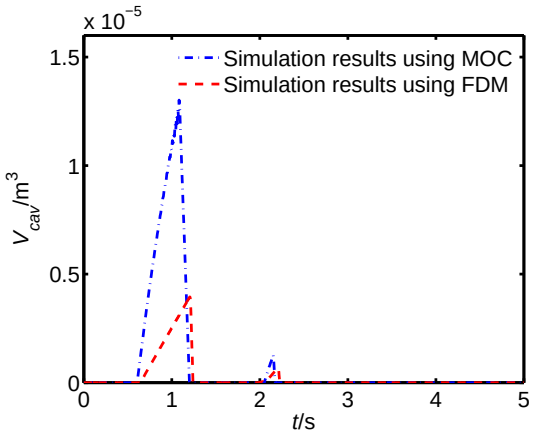

Figure 9. Simulation results of the cavitation volume in the first element between the MOC and the FDM.

As listed in Table 5, based on a comparison between Case 2 and Case 3, the durations of cavitation are much longer and the maximum cavitation volumes are larger on the downstream side of the valve. It is clear that cavitation is more likely to occur on the downstream side of the valve.

5. Conclusions

To reveal the mechanism of cavitation growth and collapse both on upstream and downstream of the water-hydraulic pipeline, this paper proposes the finite difference method (FDM) for determining the transient pressure to estimate pipeline pressure transients caused by sudden changes in fluid velocity. Firstly, the dynamic model of cavitation volume was derived during pressure transients. Then, the cavitation appearance durations and volume changes were analyzed. Furthermore, the frictional force model with the steady and frequency-dependent unsteady items were constructed in the proposed dynamic model. By referring to experimental results in [35,37], the simulation results of two computation methods were verified to indicate that the proposed FDM for transient pressure estimation has the following two advantages:

(i) The FDM is consistent with experimental results, which is improvement over the MOC in terms of the phase differences and magnitudes of the pressure peaks.

(ii) The FDM estimates not only the magnitudes of the pressure peaks but also the changes in cavitation volume to adapt the transient pressure both with and without cavitation. By statistical results, the IAD values of the FDM are much more favorable than that of the MOC.

However, the aforementioned discussion assumes that no air is released during cavitation. In fact, water usually contains some dissolved air or gas. If the pressure declines under the saturation pressure, especially under vapor pressure with agitation, then a certain amount of air will be released as gas bubbles. Thus, these effects of gas bubbles on pressure transients with cavitation will be investigated in the near future.

Acknowledgments: The authors are grateful to the anonymous reviewers and the editor for their constructive comments. This research was supported by the National Natural Science Foundation of China (51205045, 61305092, 51775089) and the Open Foundation of the State Key Laboratory of Fluid Power & Mechatronic Systems (GZKF-201515).

Author Contributions: Dan Jiang conceived and designed the structure of this paper; Tianyang Zhao and Wenzhi Cao performed the simulation; Cong Ren reviewed the literature.

Conflicts of Interest: The authors declare no conflict of interest.

Abbreviation

IAD	Integral of absolute difference
B_{eff} (Pa)	Effective bulk modulus
c_0 (m/s)	Acoustic velocity in the fluid
f	Coefficient of Darcy–Weisbach
F_0 (N)	Steady friction
$F(q)$ (N)	Friction
m_i	Weighting constant
n_i	Weighting constant
p	Vector of pressures at nodes
p_A, p_B, p_P (Pa)	Pressure at points A, B, and P
p_{resu} (Pa)	Pressure in the upstream tank
p_{resd} (Pa)	Pressure in the downstream tank
p'	New vector of pressures at nodes
p_{Lexp}	Experimental results of pressure transients at the valve
p_{Lss}	Steady-state pressure at the valve
p_{Lth}	Simulation results of pressures transients at the valve
q	Vector of flow rate at nodes

q_A, q_B, q_P (m^3/s)	Flow rate at points A, B, and P
q'	New vector of flow rate at nodes
q_{in} (m^3/s)	Inflow rate
q_{out} (m^3/s)	Outflow rate
r_0 (m)	Radius of the pipeline
v (m/s)	Velocity in the fluid
v_0 (m/s)	Initial velocity in the fluid
V_{cav} (m^3)	Cavitation volume
Y_i (N)	Weighting function
ρ (kg/m^3)	Density of fluid
μ (Pa · s)	Viscosity of fluid

References

1. Kojima, E.; Shinada, M.; Shindo, K. Fluid transient phenomena accompanied with column separation in fluid power pipeline. *Bull. JSME* **1984**, *27*, 2421–2429.
2. Chaudhry, M.H.; Bhallamudi, S.M.; Martin, C.S.; Naghash, M. Analysis of transient pressures in bubbly, homogeneous, gas-liquid mixtures. *J. Fluids Eng.-Trans. ASME* **1990**, *112*, 225–231.
3. Chaudhry, M.H. *Applied Hydraulic Transients*, 3rd ed.; Springer: New York, NY, USA, 2014.
4. Guo, Q.; Zhang, Y.; Celler, B.G.; Su, S.W. Backstepping control of electro-hydraulic system based on extended-state-observer with plant dynamics largely unknown. *IEEE Trans. Ind. Electron.* **2016**, *63*, 6909–6920.
5. Guo, Q.; Zhang, Y.; Celler, B.G.; Su, S.W. State-constrained control of single-rod electrohydraulic actuator with parametric uncertainty and load disturbance. *IEEE Trans. Control Syst. Technol.* **2017**, doi:10.1109/TCST.2017.2753167.
6. Guo, Q.; Wang, Q.; Liu, Y. Anti-windup control of electro-hydraulic system with load disturbance and modeling uncertainty. *IEEE Trans. Ind. Inform.* **2017**, doi:10.1109/TII.2017.2768106.
7. Guo, Q.; Yu, T.; Jiang, D. Robust H_∞ positional control of 2-DOF robotic arm driven by electro-hydraulic servo system. *ISA Trans.* **2015**, *59*, 55–64.
8. Shu, J.J.; Burrows, C.R.; Edge, K.A. Pressure pulsation in reciprocating pump piping systems Part 1: Modelling. *Proc. Inst. Mech. Eng. Part I* **1997**, *211*, 229–237.
9. Shu, J.J. A finite element model and electronic analogue of pipeline pressure transients with frequency-dependent friction. *J. Fluids Eng.* **2003**, *125*, 194–199.
10. Shu, J.J. Modeling vaporous cavitation on fluid transient. *Int. J. Press. Vessels Pip.* **2003**, *80*, 187–195.
11. Bergant, A.; Simpson, A.R. Pipeline column separation flow regimes. *J. Hydraul. Eng.* **1999**, *125*, 835–848.
12. Bergant, A.; Simpson, A.R.; Tijsseling, A.S. Waterhammer with column separation: A historical review. *J. Fluids Struct.* **2006**, *22*, 135–171.
13. Jiang, D.; Li, S.J. Simulation of hydraulic pipeline pressure transients accompanying cavitation and gas bubbles using Matlab/Simulink. In Proceedings of the 2006 ASME Joint U.S.-European Fluids Engineering Summer Meeting, Miami, FL, USA, 17–20 July 2006; pp. 657–665.
14. Jiang, D.; Li, S.J.; Bao, G. Parameter identification of gas bubble model in pressure pulsations using genetic algorithms. *Acta Phys. Sin.* **2008**, *57*, 5072–5080.
15. Jiang, D.; Li, S.J.; Edge, K.A.; Zeng, W. Modeling and simulation of low pressure oil-hydraulic pipeline transients. *Comput. Fluids* **2012**, *67*, 79–86.
16. Jiang, D.; Li, S.J.; Yang, P.; Zhao, T.Y. Frequency-dependent friction in pipelines. *Chin. Phys. B* **2015**, *24*, 034701.
17. Shi, Y.; Wang, Y.; Cai, M.; Zhang, B.; Zhu, J. An aviation oxygen supply system based on a mechanical ventilation model. *Chin. J. Aeronaut.* **2018**, *31*, 197–204, doi:10.1016/j.cja.2017.10.008.
18. Shi, Y.; Zhang, B.; Cai, M.; Zhang, D. Numerical Simulation of volume-controlled mechanical ventilated respiratory system with two different lungs. *Int. J. Numer. Methods Biomed. Eng.* **2016**, 33, 2852, doi:10.1002/cnm.2852.
19. Shi, Y.; Zhang, B.; Cai, M.; Xu, W. Coupling Effect of Double Lungs on a VCV Ventilator with Automatic Secretion Clearance Function. *IEEE/ACM Trans. Comput. Biol. Bioinform.* **2017**, doi:10.1109/TCBB.2017.2670079.
20. Shi, Y.; Wu, T.; Cai, M.; Wang, Y.; Xu, W. Energy conversion characteristics of a hydropneumatic transformer in a sustainable-energy vehicle. *Appl. Energy* **2016**, *171*, 77–85.

21. Sadafi, M.; Riasi, A.; Nourbakhsh, S.A. Cavitating flow during water hammer using a generalized interface vaporous cavitation model. *J. Fluids Struct.* **2012**, *34*, 190–201.
22. Karadžić, U.; Bulatović, V.; Bergant, A. Valve-Induced Water Hammer and Column Separation in a Pipeline Apparatus. *J. Mech. Eng.* **2014**, *60*, 742–754.
23. Iglesias-Rey, P.L.; Fuertes-Miquel, V.S.; Garcia-Mares, F.J.; Martínez-Solano, F.J. Characterization of Commercial Air Intake and Exhaust Valves. *Tecnol. Cienc. Agua* **2016**, *7*, 57–69.
24. Fuertes-Miquel, V.S.; López-Jiménez, P.A.; Martínez-Solano, F.J.; López-Patiño, G. Numerical modelling of pipelines with air pockets and air valves. *Can. J. Civ. Eng.* **2016**, *43*, 1052–1061.
25. Majd, A.; Ahmadi, A.; Keramat, A. Investigation of Non-Newtonian Fluid Effects during Transient Flows in a Pipeline. *J. Mech. Eng.* **2016**, *62*, 105–115.
26. Zhou, L.; Wang, H.; Liu, D.Y.; Ma, J.J.; Wang, P.; Xia, L. A second-order Finite Volume Method for pipe flow with water column separation. *J. Hydro-Environ. Res.* **2017**, *17*, 47–55.
27. Wang, H.; Zhou, L.; Liu, D.Y.; Karney, B.; Wang, P.; Xia, L.; Ma, J.J.; Xu, C. CFD Approach for column separation in water pipelines. *J. Hydraul. Eng.* **2016**, *142*, 04016036.
28. Himr, D. Investigation and numerical simulation of a water hammer with column separation. *J. Hydraul. Eng.* **2016**, *141*, 04014080
29. Wylie, E.B.; Streeter, V.L.; Suo, L.S. *Fluid Transients in Systems*; Prentice-Hall: Englewood Cliffs, NJ, USA, 1993.
30. Pettersson, M.; Weddfelt, K.; Palmberg, J.O. Modelling and measurement of cavitation and air release in a fluid power piston pump. In Proceedings of the Third Scandinavian International Conference on Fluid Power, Linköping, Sweden, 25–26 May 1993; p. 113.
31. Harris, R.M.; Edge, K.A.; Tillley, D.G. The suction dynamics of positive displacement axial piston pumps. *J. Dyn. Syst. Meas. Control* **1994**, *116*, 281–287.
32. Zielke, W. Frequency-dependent Friction in Transient Liquid Flow. *J. Basic Eng.* **1968**, *90*, 109–115.
33. Trikha, A.K. Efficient Method for Simulation Frequency-dependent Friction in Transient Liquid Flow. *J. Fluids Eng.* **1975**, *97*, 97–105.
34. Taylor, S.E.M.; Johnston, D.N.; Longmore, D.K. Modeling of transient flow in hydraulic pipelines. *Proc. Inst. Mech. Eng. Part I* **1997**, *211*, 447–456.
35. Vitkovsky, J.P.; Bergant, A.; Simpson, A.R.; Martin M.A.; Lambert, F. Systematic evaluation of one-dimensional unsteady friction models in simple pipelines. *J. Hydraul. Eng.* **2006**, *132*, 696–708.
36. Rabie, M.G.; Rabie, M. *Fluid Power Engineering*; McGraw-Hill Education: New York, NY, USA, 2009.
37. Sanada, K.; Kitagawa, A.; Takenaka, T. A study on analytical methods by classification of column separations in a water pipeline. *Bull. JSME* **1990**, *56*, 585–593.